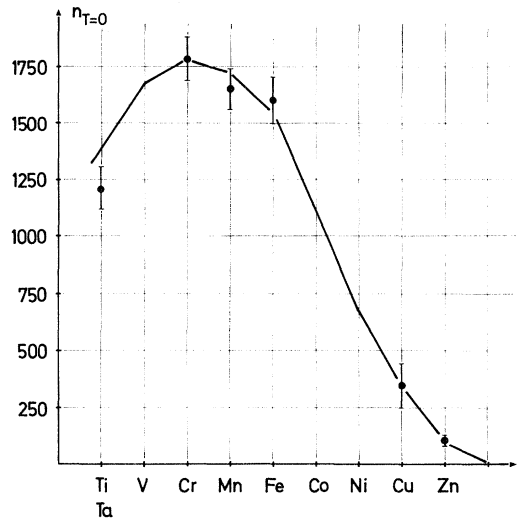

FIG. 3. Wipeout numbers extrapolated to $T=0$°K for $3d$ transition-metal impurities in aluminum.

The measured temperature dependence of the charge-density oscillation, in our opinion, is brought about by the localized spin fluctuations at the impurity sites. The localized spin fluctuations manifest themselves through the temperature dependence of the impurity density of states at the Fermi level. It is worth mentioning, however, that the whole problem can be formulated also in a little bit different way by replacing $V_{\vec{k}d}G_d{}^{\sigma}(i\omega_n)V_{\vec{k}'d}$ in Eq. (4) by a temperature-dependent scattering amplitude $t_{\vec{k}\vec{k}'}{}^{\sigma}(i\omega_n)$. It has already been suggested[19] that in the Kondo model the scattering amplitude behaves like $t_{\vec{k}\vec{k}'}{}^{\sigma}(T;\mu+i\delta)=t_{\vec{k}\vec{k}'}{}^{\sigma}(0;\mu+i\delta)[1-\text{const}T^2]$. So the effect reported here, in principle, can also be explained quantitatively in terms of the Kondo model. Unfortunately, in the framework of the Kondo model, one cannot give a numerical estimation of $\tilde{\Theta}$.

Helpful discussions during this work with Dr. A. Jánossy, Dr. K. Tompa, and Dr. A. Zawadowski are gratefully acknowledged. The authors were happy to have a fruitful discussion on this subject with Professor A. Blandin, Professor F. Gautier, and Dr. H. Launois. We are grateful to Dr. E. Csetényi and Dr. C. R. Vassel for supplying the samples and to Mr. P. Bánki for helping with the measurements.

[1]J. Friedel, Can. J. Phys. 34, 1190 (1956), and Nuovo Cimento Suppl. 7, 287 (1958).
[2]W. Kohn and S. H. Vosko, Phys. Rev. 119, 912 (1960)
[3]A. Blandin and J. Friedel, J. Phys. Radium 21, 689 (1960).
[4]P. W. Anderson, Phys. Rev. 124, 41 (1961).
[5]J. M. Brettel and A. J. Heeger, Phys. Rev. 153, 319 (1967).
[6]G. Grüner, E. Kovács-Csetényi, K. Tompa, and C. R. Vassel, to be published.
[7]D. C. Langreth, Phys. Rev. 150, 516 (1966).
[8]K. Tompa, G. Grüner, A. Jánossy, and F. Tóth, Solid State Commun. 8, 78 (1969).
[9]A. Jánossy, to be published.
[10]P. G. de Gennes, J. Phys. Radium 23, 630 (1968).
[11]D. L. Mills and P. Lederer, Phys. Rev. 165, 837 (1968); M. J. Levine and H. Suhl, Phys. Rev. 171, 567 (1968); M. J. Levine, T. V. Ramakrishnan, and R. A. Wiener, Phys. Rev. Lett. 20, 1370 (1968); N. Rivier and M. J. Zukermann, Phys. Rev. Lett. 21, 904 (1968).
[12]A. A. Abrikosov, L. P. Gor'kov, and I. E. Dzyaloshinski, in *Methods of Quantum Field Theory in Statistical Physics*, translated and edited by R. Silverman (Prentice-Hall, Englwood Cliffs, N. J., 1963).
[13]I. Adawi, Phys. Rev. 146, 379 (1966).
[14]C. Hargitai and G. Corradi, Solid State Commun. 7, 1535 (1969).
[15]A. D. Caplin and C. Rizzuto, Phys. Rev. Lett. 21, 746 (1968).
[16]R. Aoki and T. Ohtsuka, J. Phys. Soc. Jap. 26, 651 (1969).
[17]T. J. Rowland, Acta Met. 3, 74 (1965).
[18]K. Tompa, F. Tóth, and G. Grüner, Solid State Commun. 7, 51 (1969).
[19]A. Zawadowski, private communication.

Noncubic Magnetic Anisotropies in Flux-Grown Rare-Earth Iron Garnets

A. Rosencwaig, W. J. Tabor, F. B. Hagedorn, and L. G. Van Uitert
Bell Telephone Laboratories, Murray Hill, New Jersey 07974
(Received 9 February 1971)

Torque measurements have been performed on flux-grown magnetic garnets exhibiting strong noncubic anisotropies. The observed orthorhombic anisotropies are interpreted in terms of a growth-induced pair-ordering model.

Flux-grown magnetic garnets containing various combinations of rare earths have been recently reported[1] to exhibit uniaxial magnetic anisotropies of the order of 10^4 erg/cm^3 at room temperature. Noncubic magnetic properties reported previously[2,3] in flux-grown garnets have been attributed to strains induced either during crystalline growth or during sample preparation.

We have found that the anisotropies reported here cannot be readily expalined in terms of strains alone.

We consider in detail the noncubic anisotropy in crystals of $(Y_{0.62}Eu_{0.06}Gd_{0.17}Tb_{0.15})_3Al_{0.6}Fe_{4.4}O_{12}$. For magnetic-bubble-device applications these garnet crystals were grown by slow cooling from 1300°C in a $PbO \cdot PbF_2 \cdot B_2O_3$ flux.[4] This material was used for the present investigations because it was available in sufficient quantity and quality so that a number of different samples from several different cyrstals could be evaluated.

Garnets grow with two different types of exposed facets, one type being {110}, the other {112}. Therefore samples were obtained from both types of facets in order to characterize completely any growth-related phenomena. For this study, samples were cut from material just beneath a growth facet. Care was taken to obtain samples which grew entirely beneath a single facet by cutting only into large cyrstals.

Two representative sets of torque curves are shown in Fig. 1, one set each from {110} and {112} samples. The torque curves were obtained on a recording torque magnetometer. The noncubic magnetic anisotropy was found to be essentially of orthorhombic symmetry, and the three principal planes for each sample's anisotropy were experimentally determined. Orientation of the samples was done by conventional x-ray techniques, and the crystallographic directions indicated on the abscissas of Fig. 1 are estimated to be ±2°. Fourier analysis of the curves of Fig. 1 yielded terms of significant amplitudes with both twofold and fourfold symmetry. The fourfold term was assumed to be entirely due to the cubic cyrstalline anisotropy, with the twofold term due to both crystalline and growth-induced anisotropy.

Results from six different samples were obtained in this way and are listed in Table I. A

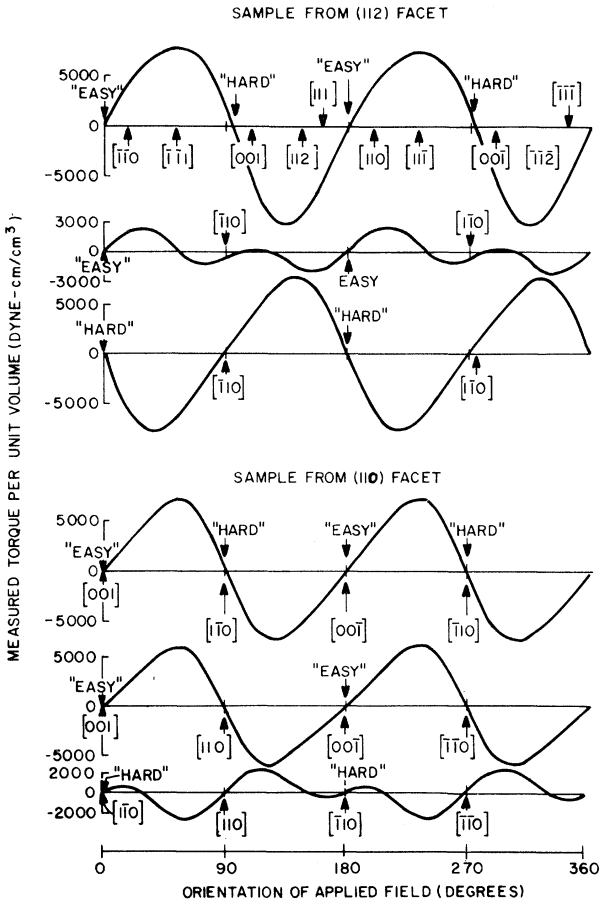

FIG. 1. Measured torques plotted as a function of applied field orientation for two different garnet samples. For all plots the field was 10 kOe. Magnetic and crystallographic axes are shown in each plot to identify the mutually orthogonal planes in which the field was rotated.

sample cut from beneath a (110) growth facet has easy and hard axes parallel to the [001] and [1$\bar{1}$0] directions in the growth plane, while the intermediate axis is parallel to the [110] direction. A sample cut from a (112) growth facet has an easy axis in the ($\bar{1}$10) plane containing the [11$\bar{1}$]

Table I. Measured anisotropies in $(Y_{0.62}Eu_{0.06}Gd_{0.17}Tb_{0.15})_3Al_{0.6}Fe_{4.4}O_{12}$.

Growth facet	Cubic anisotropy K_1 (erg/cm³)	Noncubic anisotropy energy (erg/cm³) Easy	Medium	Hard	θ (deg)
(112)	−3100	0	1200	8000	52
(112)	−3100	0	1200	7700	53
(110)	−3100	0	6200	7500	
(110)	−3500	0	7650	9200	
(110)	−3400	0	6900	10 200	
(110)	−3600	0	7500	9900	

and [112] axes, and at an angle $\theta \simeq 52°$ from the [11$\bar{1}$] toward the [112] axis. The hard axis also lies in this plane, normal to the easy axis. The intermediate axis is the [$\bar{1}$10] direction. Table I also lists the crystalline cubic anisotropy, as determined from the fourfold terms in the torque curves.

Two aspects of Table I should be emphasized: (1) The cubic anisotropies are very nearly the same for all samples and in good agreement with the total anisotropies (-3300 erg/cm^3), measured in the same samples after elimination of the noncubic anisotropy by annealing; (2) the magnitude of the growth-induced anisotropy varies from sample to sample. This variation is significantly larger than can be attributed to experimental uncertainty and suggests that the growth-induced effects may have a real variation, perhaps caused by different growth conditions. Nevertheless, the measured values in Table I are consistent enough to point to a real effect in these flux-grown garnets.

Several of the major features of this noncubic anisotropy can be understood within the framework of a model[5] based on the development of short-range ordering of cation pairs[6] during crystalline growth. Of the numerous possible pair-ordering schemes, we have considered short-range pair ordering between ions of the rare-earth sublattice and those in the iron sublattices. We consider a garnet having two types of ions, A and B, in the rare-earth sublattice and the iron ions C in the two iron sublattices. We treat the rare-earth–iron interaction in dipolar form, which accounts exactly for dipole-dipole interactions and can be considered as a first approximation to more complex mechanisms.[7-10] There are two types of relevant rare-earth–iron pair orderings. Type I involves the tetrahedral irons, while type II involves the octahedral irons. Treating only the nearest-neighbor iron ions, we find that the pair bonds of type I lie along $\langle 100\rangle$ directions and those of type II along $\langle 210\rangle$ directions.

If we assume that the preferential pair ordering is dependent on the orientation of the pair-bond direction with respect to the crystal-growth facet, we then find that the total pair anisotropy due to both type-I and -II pairs under the (110) growth facet may be written (in a coordinate system where $x \equiv [001]$, $y \equiv [1\bar{1}0]$, $z \equiv [110]$) as

$$E_{(110)} = 2(N_{AC}l_0)^{I}(\epsilon_2{}^{I}-\epsilon_1{}^{I})(\alpha_x{}^2-\tfrac{1}{3}) + \tfrac{2}{5}(N_{AC}l_0)^{II}[\epsilon_1{}^{II}(\alpha_y{}^2+9\alpha_z{}^2)+\epsilon_2{}^{II}(4\alpha_x{}^2+8\alpha_y{}^2+8\alpha_z{}^2) + \epsilon_3{}^{II}(16\alpha_x{}^2+11\alpha_y{}^2+3\alpha_z{}^2)] - \tfrac{1}{3}(N_{AC}l_0)^{II}(4\epsilon_1{}^{II}+8\epsilon_2{}^{II}+12\epsilon_3{}^{II}). \quad (1)$$

In Eq. (1) the magnetization has direction cosines $(\alpha_x, \alpha_y, \alpha_z)$, and the superscripts I and II designate the parameters for type I and II pair ordering, respectively. The total number of AC bonds per unit volume is given by N_{AC}. The term $l_0 = l_{AC} - l_{BC}$ is the pair interaction coefficient. The preference parameters $\epsilon_i{}^{I,II}$ represent the relative preference for each of the different AC bonds of types I and II. Equation (1) defines an orthorhombic growth-induced anisotropy whose principal axes of the $\{110\}$ coordinate system. This is the observed symmetry.

Similarly under the (112) growth facet we find (when in a coordinate system where $x \equiv [11\bar{1}]$, $y \equiv [\bar{1}10]$, $z \equiv [112]$) that

$$E_{(112)} = \tfrac{2}{3}(N_{AC}l_0)^{I}(\epsilon_2{}^{I}-\epsilon_1{}^{I})[\alpha_x{}^2+2\alpha_z{}^2-(2\sqrt{2})\alpha_x\alpha_z-1] + \tfrac{2}{5}(N_{AC}l_0)^{II}\{\epsilon_1{}^{II}(12\alpha_x{}^2+2\alpha_y{}^2+6\alpha_z{}^2)+\epsilon_2{}^{II}[\tfrac{2}{3}\alpha_x{}^2+4\alpha_y{}^2+\tfrac{16}{3}\alpha_z{}^2+(8\sqrt{2}/3)\alpha_x\alpha_z] + \epsilon_3{}^{II}[\tfrac{2}{3}\alpha_x{}^2+\alpha_y{}^2+\tfrac{25}{3}\alpha_z{}^2-(10\sqrt{2}/3)\alpha_x\alpha_z]+\epsilon_4{}^{II}[\tfrac{2}{3}\alpha_x{}^2+9\alpha_y{}^2+\tfrac{1}{3}\alpha_z{}^2+(2\sqrt{2}/3)\alpha_x\alpha_z]+\epsilon_5{}^{II}(6\alpha_x{}^2+4\alpha_y{}^2)\} - \tfrac{1}{3}(N_{AC}l_0)^{II}[8\epsilon_1{}^{II}+4(\epsilon_2{}^{II}+\epsilon_3{}^{II}+\epsilon_4{}^{II}+\epsilon_5{}^{II})]. \quad (2)$$

Equation (2) defines a noncubic anisotropy under the (112) growth facet with such symmetry that the easy axis will lie either along the [$\bar{1}$10] axis in the (112) plane, or alternatively somewhere in the ($\bar{1}$10) plane. This again is the observed symmetry.

It is difficult to use Eqs. (1) and (2) as they stand to make quantitative predictions because of the large number of undetermined parameters. We therefore make an assumption about the angular dependence of these parameters:

$$\epsilon_i{}^{I,II} = \epsilon_{AC}\{|\cos\theta_i| - |\sin\theta_i|\},$$

where θ_i is the angle between the ith bond direction and the growth-facet normal.[11] We now have only two independent parameters—the generalized pair interaction coefficients $(N_{AC}l_0)^{I}\epsilon_{AC}$ and

$(N_{AC}l_0)^{II}\epsilon_{AC}$.

To account for the ordering of easy, intermediate, and hard axes seen in Table I, we find from Eqs. (1) and (2) that for all of the samples, the ratio $R=(N_{AC}l_0)^{I}\epsilon_{AC}/(N_{AC}l_0)^{II}\epsilon_{AC}$ is always negative, indicating that l_0^{I} and l_0^{II} differ in sign. This result is to be expected since the pair interaction is of one sign for the ferromagnetically coupled rare-earth–octahedral-iron pairs, but of opposite sign for the antiferromagnetically coupled rare-earth–tetrahedral-iron pairs.

By dividing Eqs. (1) and (2) by $Q=(N_{AC}l_0)^{II}\epsilon_{AC}$, we obtain normalized expressions for the anisotropy energies as a function of the ratio R. The energies for the principal anisotropy axes are plotted in Fig. 2 as a function of negative R with Q negative. Also plotted for the (112) facet is the orientation of the easy axis. The data in Table I are also plotted in Fig. 2, where reasonable agreement of the relative magnitudes and orientations of the measured anisotropies with those predicted by the model is obtained for $R\simeq-8$. Fitting the data as shown implies that $[(N_{AC}l_0)^{I}\epsilon_{AC}]_{avg}\simeq 1.8\times10^{4}$ erg/cm^3 and $[(N_{AC}l_0)^{II}\epsilon_{AC}]_{avg}\simeq -0.23\times10^{4}$ erg/cm^3. It is clear, however, that a precise determination of these quantities is not warranted by the available data.

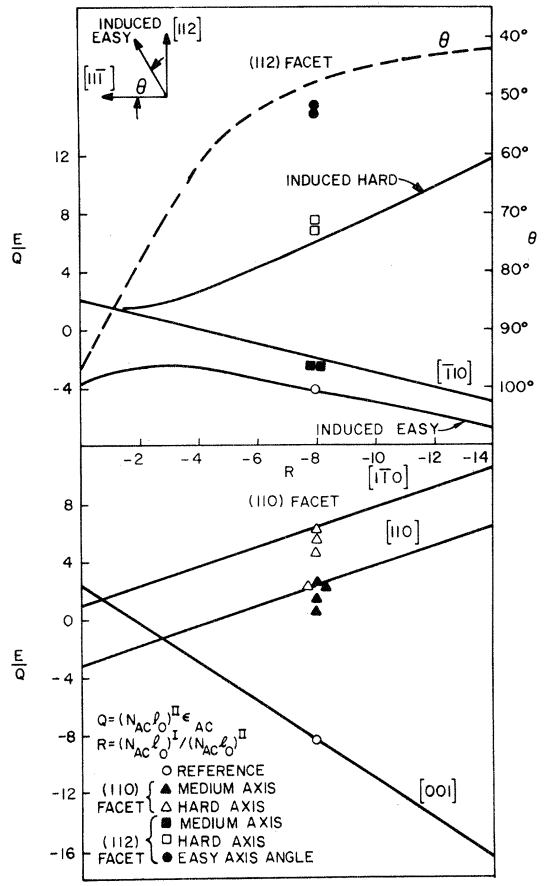

FIG. 2. Normalized induced anisotropies as predicted by the pair-ordering model plotted along the principal axes of the induced orthorhombic anisotropy energy surface, as a function of the ratio R. The orientation of the easy axis under the (112) facet is also shown. The data of Table I are plotted for $R=-8$ using the predicted easy axes as reference positions.

The major features predicted by such a model are observed experimentally: (1) the orientations of the noncubic anisotropies beneath both facets relative to the crystallographic directions; (2) the relative magnitudes of the medium and hard axes under each facet; (3) the relationship of the (110) anisotropy to that of the (112) anisotropy for the same value of R; and (4) the sign difference of l_0^{I} and l_0^{II} as reflected in the negative value of R.

Additional support for this model comes from the fact that the noncubic anisotropy disappears after annealing at temperatures above 1200°C. Thermally activated atomic diffusion would be expected to randomize those pairs ordered during crystalline growth. Finally, the model contains the flexibility to describe different observed anisotropy orientations. Preliminary results on flux-grown $(Gd_{0.78}Tb_{0.22})_3Fe_5O_{12}$ indicate that the easy axis beneath the (112) facet is at $\theta\simeq-11°$, while the easy axis beneath the (110) facet is along the $[1\bar{1}0]$ axis. One obtains this orientation in the model by changing the sign of Q, thereby interchanging the definitions in Fig. 2 of easy and hard axes, and subtracting 90° from the angle θ. Then for $R\simeq-2$ and Q positive, the model predicts the observed orientations of the easy axes in $(Gd_{0.78}Tb_{0.22})_3Fe_5O_{12}$.

Although Eqs. (1) and (2) pertain specifically to a binary rare-earth system, they apply equally to the more complicated garnets used in this study, since A in the model can represent a combination of some of the rare earths while B represents the rest. The presence of Al or Ga in the iron sublattices can give rise to preferential Al-Fe ordering. However, this pair ordering is probably less significant than the rare-earth–iron pair ordering since the higher mobility of the iron and Al ions[12] should result in little growth-induced Al-Fe ordering remaining after crystalline growth.

In conclusion, it can be readily shown that on the basis of a dipole-dipole interaction only, one needs only ~1% preferential pair ordering to produce anisotropies of the order of 10^4 erg/cm^3.

If one considers the much stronger anisotropic interactions[7-10] between rare-earth and iron ions, far less than 1% preferential pairing is probably required.

[1]A. H. Bobeck, E. G. Spencer, L. G. Van Uitert, S. C. Abrahams, R. L. Barns, W. H. Grodkiewicz, R. C. Sherwood, P. H. Schmidt, D. H. Smith, and E. M. Walters, Appl. Phys. Lett. 17, 131 (1970).

[2]A. W. Smith and G. W. Williams, Can. J. Phys. 39, 768 (1961).

[3]R. A. Lefever, K. A. Wickersheim, and A. B. Chase, J. Phys. Chem. Solids 26, 1529 (1965).

[4]L. G. Van Uitert, W. A. Bonner, W. H. Grodkiewicz, L. Pictroski, and G. J. Zydzik, Mat. Res. Bull. 5, 325 (1970).

[5]A. Rosencwaig and W. J. Tabor, in Proceedings of the Sixteenth Conference on Magnetism and Magnetic Materials, Miami, Florida, 1970 (to be published).

[6]A model based on preferential site occupation, discussed in the following Letter [A. Rosencwaig, W. J. Tabor, and R. D. Pierce, Phys. Rev. Lett. 26, 779 (1971)], gives the same results as the pair-ordering model.

[7]J. W. Henderson and R. L. White, Phys. Rev. 123, 1627 (1961).

[8]P. M. Levy, Phys. Rev. 147, 311 (1966).

[9]R. M. White and R. L. White, Phys. Rev. Lett. 20, 62 (1968).

[10]P. M. Levy, Phys. Rev. Lett. 20, 1366 (1968).

[11]The $\epsilon_i^{I,II}$ can in general be written as a series expansion in powers of $\cos\theta_i$, with only even powers permitted in a cubic crystal. The absolute-magnitude form used in this paper is one such expansion. Other simple expansions in even powers give essentially similar results.

[12]F. Euler, B. R. Capone, and E. K. Czerlinsky, IEEE Trans. Magn. 3, 509 (1967).

Pair-Preference and Site-Preference Models for Rare-Earth Iron Garnets Exhibiting Noncubic Magnetic Anisotropies

A. Rosencwaig, W. J. Tabor, and R. D. Pierce
Bell Telephone Laboratories, Murray Hill, New Jersey 07974
(Received 16 February 1971)

The pair anisotropy model is extended to include the next-nearest-neighbor tetrahedral-iron ions. An anisotropy model based on growth-induced preferential site occupation is derived using the pair model. With the site model the nearest-neighbor tetrahedral- and nearest-neighbor octahedral-iron ions lead solely to a uniaxial anisotropy under both growth facets. Inclusion of the next-nearest-neighbor tetrahedral-iron ions results in the experimentally observed orthorhombic anisotropies.

Recent experiments on flux-grown magnetic garnets containing two or more rare earths have shown that some of these garnets exhibit noncubic magnetic anisotropies of the order of 10^4 erg/cm^3 at room temperature.[1] We have earlier proposed a pair-anisotropy model[2] based on the possible existence of a growth-induced preferential pair ordering between the rare-earth ions and their nearest-neighbor tetrahedral-iron (NNT) and nearest-neighbor octahedral-iron (NNO) ions. This model has been shown to predict the observed symmetries of the noncubic anisotropies,[2] and to give good quantitative agreement with room-temperature torque measurements recently performed on a series of these garnets.[3]

In this Letter we extend the pair model to include the next-nearest-neighbor tetrahedral-iron (NNNT) ions as well. Although the NNNT ions are farther from the rare-earth site than the NNT ions, the anisotropic superexchange between the rare earths and the NNNT ions is comparable to if not larger than that with the NNO ions.[4,5] In addition we derive, with help of the pair-preference model, a site-preference model in which we assume a growth-induced preferential site occupation of the rare-earth ions in the dodecahedral sublattice. We show that, unlike the pair-preference model, the site-preference model predicts only a uniaxial anisotropy when the NNNT ions are not considered. However, when these ions are considered, the site-preference model predicts the same orthorhombic symmetries for the induced anisotropies as does the pair-preference model.

We consider a garnet crystal having two rare-earth ions, A and B, in the dodecahedral sublattice and the iron ions C in the tetrahedral and octahedral sublattices. Each rare-earth ion is bonded to (i) two NNT ions by $\langle 100\rangle$ bonds, (ii) four NNO ions by $\langle 210\rangle$ bonds, and (iii) four NNT ions